# Theoretical study of the formation of $C_{18}H$ and $C_{18}H_2$ molecules by low energy irradiation with atomic and molecular hydrogen

F. J. Domínguez-Gutiérrez[a,*], C. Martínez-Flores[b], P. S. Krstic[c], R. Cabrera-Trujillo[d,e], U. von Toussaint[a]

[a] *Max-Planck-Institut für Plasmaphysik, Boltzmannstrasse 2, 85748 Garching, Germany*
[b] *Departamento de Química, División de Ciencias Básicas e Ingeniería, Universidad Autónoma Metropolitana-Iztapalapa, San Rafael Atlixco 186, Col. Vicentina, Iztapalapa C. P. 09340, Ciudad de México, México.*
[c] *Institute for Advanced Computational Science, Stony Brook University, Stony Brook, NY 11749, USA.*
[d] *Instituto de Ciencias Físicas, Universidad Nacional Autónoma de México, Ap. Postal 43-8, Cuernavaca, Morelos, 62251, Mexico.*
[e] *Theoretische Chemie, Physikalisch-Chemisches Institut, Universität Heidelberg, INF 229, 69120 Heidelberg, Germany*

**Abstract**

We study the formation of $C_{18}H$ and $C_{18}H_2$ by irradiating a cyclo[18]carbon molecule with atomic and molecular hydrogen at impact energy, $E$, in the range of 0.5-25 eV. We utilize the density-functional tight-binding method to perform molecular dynamics simulations to emulate the interaction of a carbon ring when colliding with atomic or molecular hydrogen. From our results, the formation of the $C_{18}H$ molecules is likely to occur upon irradiating by H atoms at $E < 10$ eV and by $H_2$ molecules at $2 < E < 15$ eV center of mass energy. Formation of $C_{18}H_2$ molecules is only observed at around $E = 2$ eV. Our results show that the absorption of hydrogen is more prone in atomic than in molecular hydrogen atmosphere. Thus, we find that the probability of physio-absorption reaches up to 80 % for atomic projectiles with $E < 5$ eV but only up to 10 % for the molecular ones. Our analysis shows that the deformation of the carbon ring due to the hydrogen bonding produces transition from $sp$ to $sp^2$ hybridization. The angle between the carbon atoms at the locations near to the H bond in the resulting ring is not $120^o$ but instead $110^o$ degrees. No molecular fragmentation of the $C_{18}$ ring is observed.

## 1. Introduction

The electronic structure of carbon atoms produces various allotropic forms. These forms include, for example, ball shapes of buckminsterfullerene, nanotubes, nanobuds, nanoribbons and 2D structures such as graphene. More unusual forms of carbon exist, one of them being just recently reported by Kaiser et al. [1]. This allotrope is a ring of eighteen carbon atoms, named cyclo[18]carbon or $C_{18}$. The C atoms are connected by alternating triple and single bonds, forming a polyyne and a cyclocarbon. The various allotropic forms are a distinctive feature of the $sp$-hybridization of carbon valence electrons. Hückel's rule predicts an aromatic structure with no bond length alternation for planar, cyclically conjugated systems with $(4m+2)$ $\pi$-electrons, where $m$ is a natural number related to $C_N$ carbon rings with $N = 4m+2$ as the number of C atoms [2]. Hoffmann predicted double aromatic stabilization consequence of two orthogonal ring currents in $C_{18}$ [3]. Thus, a theoretical debate started on the chemical structure of cyclo[$N$]carbons with conclusions which have, so far, depended on the theoretical approach. Most of the density functional theory (DFT) and Møller-Plesset perturbation theory calculations predict that the lowest-energy geometry of $C_{18}$ is cumulenic $D_{18h}$ [4, 5]. Hartree-Fock, Quantum Monte Carlo, and coupled cluster methods predict that the polyyne $D_{9h}$ form is the ground state [6, 7, 8, 9, 10]. Recently, it has been found that $C_{18}$ is the smallest among carbon electron acceptor molecule reported so far [11] and its synthesis [1] paves the way for the creation of various 2D materials based on molecular carbon allotropes. For example, $C_{18}$ might

*Corresponding author: javier.dominguez@ipp.mpg.de

be used to produce graphdiyne (GDY) [12, 13]. GDY is of interest for atom catalyst where the hydrogen evolution reaction at room temperature is observed during its synthesis with zero-valent Mo atoms [14]. This catalytic process can be applied for hydrogen production with application on energy storage. The material has a porous structure that allows adsorption and diffusion of atoms, a highly desirable feature for the design of next-generation batteries. Because of the presence of a natural band gap and high degree of conjugation, GDY is also a promising material for nanoelectronics applications. Therefore, the study of the formation of $C_{18}$ molecules, with or without hydrogen atom or molecules, is needed to understand the *sp*-$sp^2$-hybridized carbon atoms formed by inserting diacetylenic ($C_4H_2$) linkages between two benzene rings in a graphene structure [15]. The formation of the $C_{18}H_n$ ($n = 1, 2, \ldots, 36$) molecules leads to anisotropy in the optical activity of the original $C_{18}$ molecule, where the molecular geometry changes can be related to transition magnetic and electric dipole moments [16].

The previous discussion sets the stage and motivates our quantum chemistry theoretical study: the absorption of hydrogen atoms by a $C_{18}$ molecule irradiated by atomic and molecular hydrogen. Our goal is to provide an insight in the formation of $C_{18}H$ and $C_{18}H_2$ and its molecular geometry modifications leading to a better understanding of this ring molecule in the development of hydrogen nano sensors. This requires a computationally expensive methodology to obtain results with chemical accuracy. The hydrogen uptake rates are highly dependent on the potential barriers and adsorption energies requiring a statistical approach to take into account all the possible projectile trajectories, which lead to the formation of a $C_{18}H$ molecule. Consequently, the Density Functional Theory (DFT) method is an ideal first candidate that provides accurate information about the electronic structure of the $C_{18}$ molecule and the *sp*- hybridization when the H atom is bound to a C atom in the $C_{18}$ ring. However, the H adsorption and scattering processes have a time scale that goes from femto to pico seconds [17]. This is a formidable computational task for the quantum-classical molecular dynamics simulation based on DFT and Carr-Parinello frameworks. These approaches require the need of a short time step (0.05 fs) with thousands of time steps to model the interaction between a carbon ring with an atomic or molecular projectile in order to track properly the formation of $C_nH_m$ molecules (here $n$ and $m$ are integer numbers). Instead, in this work, we use the less expensive semi-classical Molecular Dynamics (MD) approach based on the computationally affordable density-functional tight-binding (DFTB) method [18, 19], as implemented in the dftb+ code [20]. This method has the capability to compute energy contribution arising from large interatomic distances, spin effects, electron-electron repulsion terms, and 3-body dispersion correction and with a numerical accuracy close to those obtained by DFT simulations. Thus, in this work, we perform MD simulations to estimate the probability of formation of a $C_{18}H_X$ molecule and to analyze the mechanisms of H capture by the carbon ring in the impact energy range of 0.5 to 25 eV for 100 fs. This analysis could elucidate the feasibility for designing a fast and sensitive hydrogen nano sensor device.

Our paper is organized as follows: In Sec. 2, we briefly discuss the numerical method used in our work, as well as computation of the H-$C_{18}$ potential energy curves. In Sec. 3, we report the results of our simulations. Our concluding remarks are given in Section 4.

## 2. Computational methods

### *2.1. SCC-DFTB method*

DFTB is approximately 100 times more expensive than classical force fields approaches and up to 100 times cheaper than density functional theory. Thus, it fills the gap between classical force fields and density functional theory and is an attractive candidate for direct molecular dynamics simulations of bulk phase and condensed matter [18, 19, 21, 22]. DFTB is an approximate density functional theory in which only valence electrons are treated quantum mechanically while all core electrons and nuclei are approximated via pairwise interatomic repulsive potential.

The energy of the system is described by

$$E = \sum_i 2 f_i \langle \phi_i | H_{core} | \phi_i \rangle + \frac{1}{2} S \sum_{\substack{A,B \\ A \neq B}} \gamma^{AB} \Delta q^A \Delta q^B + \sum_{A>B}^{Atom} E_{rep}^{AB} + \frac{1}{2} S \left( \sum_{l' \in A} W_{All'} m_{Al'} + \sum_{l'' \in B} W_{Bl'l''} m_{Bl''} \right) . \quad (1)$$

where $f_i$ is an occupation number (typically 0 or 1) and $i$ runs over all molecular orbitals. The first term describes the interaction of valence electrons with core ions (nuclei and core electrons). The second term is responsible for the electron-electron interaction. The symbols $\Delta q^A$ ($\Delta q^B$) and $\gamma^{AB}$ are, respectively, a charge at center $A$ ($B$) and a chemical hardness-based parameter describing electron-electron interactions between centers $A$ and $B$; $\gamma^{AB}$ depends on the interatomic distance; and the matrix $S$ is the overlap term. The third term describes the interaction between core ions and is obtained from a fit. An important feature of DFTB that is often missing in standard DFT is a correct Coulomb asymptotic behavior for the interaction of charged molecules [19, 21]. This is due to the fact that $\gamma^{AB}$, in the electron-electron repulsion term, behaves as $1/R_{AB}$ for large interatomic distances. The last term corresponds to the spin contribution and depends on the spin channel, $\sigma$. Here, the spin coupling constant $W_{All'}$ defines the spins interaction where $l$ and $l'$ are shells on the same atom. The spin polarization $m_{Al'}$ is the difference between the Mulliken charges with spin up and down of the atom and is given as $m_{Al'} = q_{Al\uparrow} - q_{Al'\downarrow}$ [18]. DFTB provides also inexpensive tools for the description of lowlying excitations. Higher energy electronic excitations are less reliable. This limitation is a result of inherently minimal basis set (Slater type orbitals). Higher energy excitations can be included through all electrons DFT approaches and extended basis set. The DFTB approach, as implemented in the publicly available dftb+ code [18, 20] version 19.1, is used in this work. Molecular Dynamics simulations are performed by using the DFTB method with a velocity-Verlet algorithm [18, 19, 21, 22].

### *2.2. Potential energy curves*

As a first step in our study, we calculate the adiabatic potential energy curves of H and $H_2$ interacting with $C_{18}$. The absorption of H is strongly dependent on the electronic structure of the $C_{18}H$ system. We need a correct set of Slater-Koster (SK) parameters. For this purpose, we tested various SK parameter sets from the literature [18, 23, 24, 25] implemented in the DFTB+ code, in order to select the most suitable one for our systems. With appropriate well-chosen SK parameters, one should be able to model the *sp* hybridization in the $C_{18}H$ in good agreement with DFT calculations. Our first choice is the semi-relativistic, self-consistent charge set of SK parameters for materials science (MATSCI), which was successfully used to study the formation of 2D Covalent Organic Frameworks [23]. We utilized these parameters in our previous work for the study of electronic properties of a borophene sheet [26] and hydrogen uptake by carbon, boron doped carbon fullerenes [27], and C/B-N nanotubes [28]. Our second choice is the set of parameters for solid-state systems (PBC) [24] that has been used to study SiC properties and could be applied to organic systems. As a third option, we consider the long-range corrected SK parameters for bio and organic molecules [29] (OB2), which have been used in our previous work for the study of the effects of hydrogen radiation on a glycine molecule [30]. In order to explore the advantages of the inclusion of the third order corrections of the DFT energy expansion into the DFTB approach [21], we also use the SK parameters called 3OB [25] that are focused on the study of small organic molecules. The choice of these parameters reflects the fact that the 3OB were generated to improve hydrogen binding energies, proton affinities, and proton transfer barriers. To include the van der Waals interaction between H and C in our computations, we use the following three different levels of theory for the dispersion corrections: the Slater-Kirwood polarizable atomic model (SKirk) [31], the Lennard-Jones potential with parameters taken from the Universal Force-Field (UFF) [32], and the 3-body term, included through a damped pairwise London-type correction (DFT-D3) [33].

In Table 1, the bond lengths of the ground state geometry configuration of $C_{18}$ are given in units of Å, as obtained by DFTB showing good agreement to the DFT results of Kaiser et al [1]. As a consequence of the *sp* hybridization, we find that the $C_{18}$ molecule has an alternating bond length resulting of single and

Table 1: Carbon bond lengths in the $C_{18}$ molecule obtained after an optimization procedure by the DFTB method and are compared to the DFT data of Kaiser et al. [1]. We report values by using MATSCI, PBC, OB2, and 3OB SK parameters for the DFTB calculations.

| | Length (Å) | | | | |
|---|---|---|---|---|---|
| Bond | MATSCI | PBC | OB2 | 3OB | DFT[1] |
| C(1)–C(2) | 1.25 | 1.25 | 1.27 | 1.25 | 1.20 |
| C(1)–C(3) | 1.35 | 1.35 | 1.35 | 1.35 | 1.34 |

triple bonds between the carbon atoms forming the ring. We report these alternating bonding lengths by considering a system of three carbon atoms C(2)-C(1)-C(3). We find that in general all the SK parameters, i.e. MATSCI, PBC, OB2, and 3OB, produce the same geometry of the ring molecule. This confirms the $D_{9h}$ symmetry of this molecule [7, 8, 9, 10] for all cases.

In order to calculate the potential energy curves (PECs) of a $C_{18}H$ and $C_{18}H_2$, the systems consisting of $C_{18}$ ring and H or $H_2$ are first considered. The PECs are calculated as $\Delta E(r) = E_{HC}(r) - E_H - E_C$, where $E_{HC}$ is the total electronic energy of the $C_{18}H_X$ system. $E_H$ is the energy of the isolated H or $H_2$ and $E_C$ is the energy of the isolated $C_{18}$ ring. All the atomic nuclei are fixed during the energy calculations while the radial directions are chosen with respect to different adsorbate sites. We consider absorbate sites that determine the $D_{18h}$ or $D_{9h}$ symmetry axis of the ring where the H atom or $H_2$ molecule is placed at several positions on a straight line parallel to the x-y plane starting at the center of the $C_{18}$ molecule on the direction going through the C(1)-C(2), C(1)-C(3) bonds, in the radial directions toward the center of the ring, and in the plane of the ring and the C atoms location. We compute the PECs with the DFTB+ code considering the MATSCI, PBC, OB2, and 3OB SK parameters with UFF, Slater-Kirwood, and DFT-D3 dispersion corrections, which help us to select the set of SK parameters to perform MD simulations.

### *2.3. Irradiation on $C_{18}$ by Atomic and Molecular Hydrogen*

The study of the formation of a $C_{18}H$ or $C_{18}H_2$ molecule is carried out by performing molecular dynamics simulations using the DFTB approach. The center of the carbon ring is placed at the origin of the Cartesian coordinate system, then the ring is energy optimized and thermalized to 300 K using a Nose-Hoover thermostat [34] prior to hydrogen irradiation. We consider the following impact energies: 0.5, 1, 2, 5, 10, 15, 20, and 25 eV with a commensurate velocity given by $v = \sqrt{(2E/m)2}$, where $E$ is the impact energy and $m$ is the mass of the projectile. We irradiate the $C_{18}$ molecule with 942 hydrogen atoms for the atomic case and with 471 $H_2$ molecules for the molecular case. The initial H and $H_2$ positions start at a distance of 15 Å measured from the origin of our coordinate system and are randomly distributed in a target area of 1 $nm^2$ considering a spherical geometry [27] with the azimuth angle being in a range of $0 \leq \varphi \leq \pi/2$ and the zenith angle, defined in the range $-\pi/2 \leq \Theta \leq \pi/2$. The irradiation occurs atom per atom (or molecule) rather than in a cumulative process and a thermostat is not used during the MD simulations for collision dynamics. The initial velocity of the projectiles is oriented to the center of the $C_{18}$ molecule for all the cases. In Fig. 1 a), we show the initial positions of the $H_2$ molecules (represented by white spheres) and the $C_{18}$ molecule (depicted as gray spheres) used in this work. Each $H_2$ molecule has initially a random orientation. For the collision dynamics, we use the velocity-Verlet algorithm as implemented in the dftb+ package with a time step of $\Delta t = 0.05$ fs with the total simulation time of 100 fs. A Fermi-Dirac smearing is applied in the MD simulations with equivalent electronic temperature of 1000 K.

Once the carbon ring and the atomic or the molecular hydrogen projectiles are prepared, the MD simulations are performed with the dftb+ code. The analysis of the MD simulations is done by quantifying the number of H atoms, $N^{a,s}$, that are absorbed, $a$, or scattered, $s$, by the carbon ring. From the output file of our simulations, we compute the distance $d_f = \sqrt{x^2 + y^2 + z^2}$ from the final position of each H atom, defined by $x$, $y$, and $z$, to the center of the carbon ring. Scattered and adsorbed H atoms are shown in Fig. 1 a) by yellow spheres. Bound atoms are commonly found with $d_f < 7$ Å, and scattered atoms have a $d_f \gg 7$ Å. The adsorption and scattered probabilities are calculated as $N^{a,s}/N_T$ for each impact energy with $N_T$ defined as the total number of impinging projectiles. The scattering particles can be divided into transmitted and reflected projectiles. Thus, we compute the angle between the associated vectors to the initial $\vec{r}_i$ and final $\vec{r}_f$ positions of the H atom as angle $\theta_t = \arccos(\hat{r}_i \cdot \hat{r}_f)$, with $\hat{r}_{i,f}$ normalized vectors.

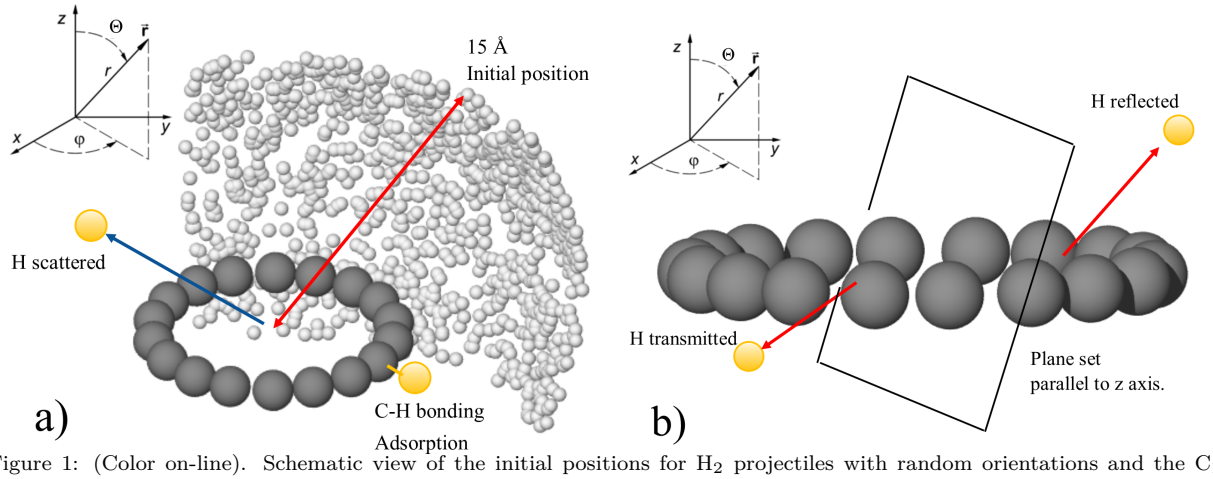


Figure 1: (Color on-line). Schematic view of the initial positions for $H_2$ projectiles with random orientations and the $C_{18}$ molecule in a). The carbon ring is set at the origin of the coordinate system, in the x-y plane. We also include a representation of the scattered and adsorbed H atom by showing them as yellow spheres. In Fig. 1 b), we show the interpretation of the transmitted and reflected H atoms by introducing a plane that divides the incident projectiles from the scattered region that is vertical along the z axis and perpendicular to the plane formed by the $C_{18}$ molecule, which determines the number of transmitted and reflected atoms. Color code: H atoms are illustrated as white(yellow) spheres, meanwhile C atoms are presented by gray spheres.

The final commensurate velocity of the projectile is computed from the output data of the MD simulations as $v_f = \sqrt{v_x^2 + v_y^2 + v_z^2}$ where $v_i$ is the final velocity component in the x, y, and z directions. In this way, H atoms with $\pi/2 < \theta_t < 3\pi/2$ and a $v_f$ similar to the initial velocity are considered as transmitted, otherwise the projectiles are identified as reflected, as shown in Fig. 1 b). The probability of these processes is calculated as $N^{\beta,t}/N_{st}$ where $N^{\beta,t}$ is the number of reflected ($\beta$) or transmitted ($t$) H atoms and $N_{st}$ is the total number of scattered H atoms. This ratio provides the probability of formation of a $C_{18}H$ or $C_{18}H_2$ molecule due to hydrogen irradiation as a function of the irradiation energy.

## 3. Results

### *3.1. Static description*

#### *3.1.1. PECs: Atomic case*

In Figs. 2 and 3, we present the PECs obtained for a hydrogen atom and a carbon ring molecule placed at a distance $r$ from the center of the ring by considering different SK parameters that describe the electronic structure of $C_{18}$ and its interaction with a H atom. In Fig. 2 a), the hydrogen atom is displaced perpendicular to the plane of the $C_{18}$ molecule passing through the center of the ring. The standard results, obtained without dispersion corrections, show that the hydrogen atom cannot be bound to the carbon ring at this adsorbate configuration. The inclusion of dispersion corrections in the computation of the PECs improves the bonding energy to 0.039 eV for the Slater Kirwood approach, 0.032 eV for the UFF, and 0.051 eV with the DFT-D3. This is still a too small binding energy to bind H at the center of the ring. In Fig. 2 b), H atoms are placed along a parallel line on the plane of the carbon ring, going through a C atom. This geometry shows different results when varying the SK parameters. MATSCI and OB2 parameters bind a hydrogen atom outside the carbon ring, at a distance of 4 Å from the origin of the ring or 0.6 Å from the carbon atom. We find that the OB2 parameters, which are obtained for biomolecules in gas phase, show the largest binding distance and energy. Since the SK parameters are obtained from different training data sets or reference molecular systems, the results vary for the bond length and binding energy. MATSCI and PBC parameters are obtained for modeling a solid-state system and cannot model properly our present cases. The DFT-D3 includes the spin-same-spin and spin-different-spin constants for all combinations of atomic shells and one-center exchange-like terms for the multicenter integrals [35]. In Fig. 2 b), we observe that the H

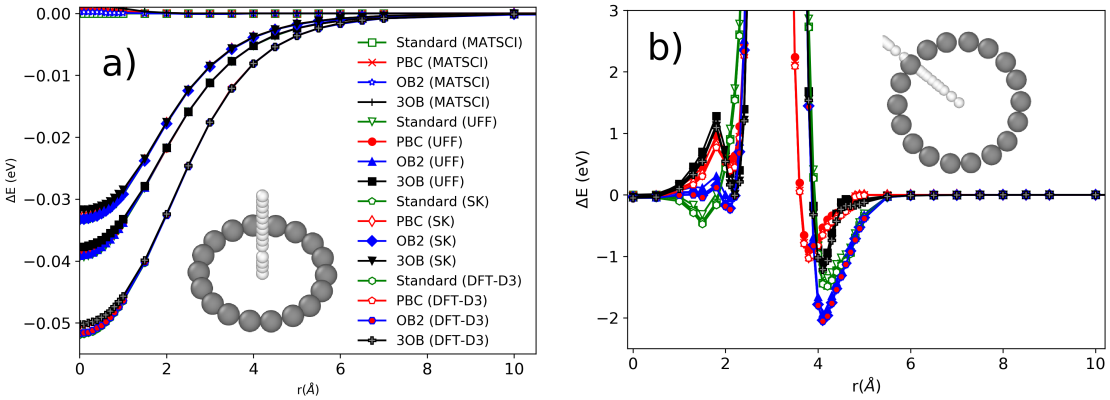


Figure 2: (Color on-line). a) Potential energy curves for the formation of a $C_{18}H$ molecule for several SK parameters sets including dispersion corrections. A schematic of the positions of the hydrogen atom and the carbon ring is shown as an inset. a) The hydrogen atom is placed along the $D_{9h}$ symmetry axis. b) The hydrogen atom is placed on the plane of the $C_{18}$ molecule and passes through a C carbon atom. (color code: white spheres represent hydrogen atoms while grey spheres represent carbon atoms.) See text for discussion.

atom is bound to the $C_{18}$ with an energy of 1 eV, which is the result of the inclusion of the DFT-D3 dispersion corrections, where the total energy of the system is expressed as $E = E_{DFTB} + E^{(2)}_{disp} + E^{(3)}_{disp}$, considering 2- and 3-body contributions in the calculations. Our results indicate that the 3OB SK parameters are a good choice to perform MD simulations to emulate the interaction of the carbon ring with the hydrogen projectile.

In Fig. 3, we show results for the PECs for the two adsorbate sites, consisting of the hydrogen atom passing through the bridge between the C(1)-C(2) and C(1)–C(3) bonds according to the $D_{9h}$ symmetry of the carbon ring. In Fig. 3a), we present the results when the H atom is placed between the line that joins the C(1)-C(3) atoms. We observe that the different SK parameter sets show differences in the PECs, but the inclusion of dispersion corrections does not affect the results. The PBC SK parameters show a repulsion of the hydrogen atom in the inner part of the carbon ring, consequently, the formation of $C_{18}H$ at the inside ring is not possible with these parameters. MATSCI SK parameters model the formation of a $C_{18}H$ with a hydrogen bonding inside and outside the carbon ring. In addition, the OB2 parameters model a $C_{18}H$ molecule with a hydrogen atom bound outside of the ring. However, the repulsion region inside the carbon ring is similar to that obtained by the PBC SK parameters. With the 3OB SK parameters, we get that H

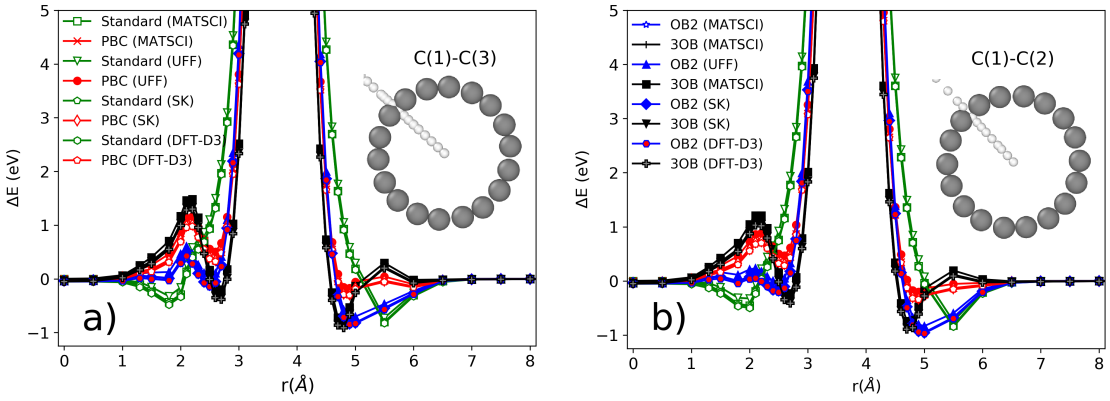


Figure 3: (Color on-line). Potential energy curves for $C_{18}$ and a H atom as a function of the distance. Here, we consider two different adsorbate sites. The hydrogen atom passes trough the bridge of the C(1)-C(3) bond in a) and C(1)-C(2) bond in b) ( shown schematically as an inset in the figure). Different SK parameters and dispersion approaches are tested. Color code and labels are the same as in Fig. 2

bounds more favorable outside of the carbon ring. Although the repulsion region inside the $C_{18}$ is similar to the results presented by OB2 and PBC, the H atom can be bound to the carbon ring in this region.

In Fig. 3 b), we present results for the adsorbate site defined in the bridge between the C(1)-C(2) carbon atoms. The results are similar to those reported in Fig. 3 a), and the hydrogen atoms can be bound to the carbon ring at the outside region. The PBC SK parameters show slight differences when comparing the C(1)-(C3) to the C(1)-C(2) bond which, in principle, reflects the proper binding of a H to the $C_{18}$ molecule resulting from a $D_{9h}$ target symmetry. In summary, the H atom is more likely to be bound to a C atom to form a $C_{18}H$ molecule.

### *3.1.2. PECs: Molecular case*

We compute the PECs of the interaction of a $H_2$ molecule at different adsorbate sites of the $C_{18}$ molecule by considering two orientations of the $H_2$ molecule, one horizontal and the other vertical with respect to the plane of the ring molecule. The center of mass of the hydrogen molecule is set at different locations along a line that goes through the center of the carbon ring. In Fig. 4, we present the PEC results by using the same MATSCI, PBC, OB2, and 3OB SK parameters with UFF and DFT-D3 dispersion corrections for a $H_2$. Here, the center of mass of the hydrogen molecule follows a line perpendicular to the plane formed by the carbon ring. The inset Fig. 4 a-b) shows two different orientation of the $H_2$ molecule, where white spheres represent a hydrogen molecule with an orientation parallel ($\parallel$) to the carbon ring plane, while silver spheres show a $H_2$ molecule perpendicular ($\perp$) to the $C_{18}$ molecule plane. Hydrogen bonding corrections [36] are included during the computation of the PECs. Both orientations of the hydrogen molecule present a bonding energy of 0.08 eV for the UFF dispersion, as shown in Fig. 4a). While an energy bonding of 0.07 eV is obtained by the DFT-D3 results in the PECs plotted in Fig. 4b). Both orientations of the hydrogen molecule are favorable for binding $H_2$ to the $C_{18}$ molecule at this adsorbate site.

In Fig. 4 c-d), PECs for three different adsorbate sites are presented. We do not find significant differences between the results for the two orientations of the $H_2$ molecule. Thus, we present only results for the perpendicular orientation case. Fig. 4c) shows results obtained by using UFF dispersion corrections reporting a small energy bonding of 0.02 eV outside of the carbon ring (at a distance of 0.6 Å from the C atom) for most of the SK utilized in the calculations. Fig. 4 d) presents results for the DFT-D3 dispersion corrections and hydrogen-hydrogen repulsion contributions. MATSCI and OB2 SK parameters results are affected by the inclusion of DFT-D3, as observed by the comparison to the results obtained with UFF corrections. Also, MATSCI and OB2 SK parameters yield that the $H_2$ molecule can be bound at both sides of the carbon ring. The 3OB SK parameters results with DFT-D3 dispersion corrections show similar

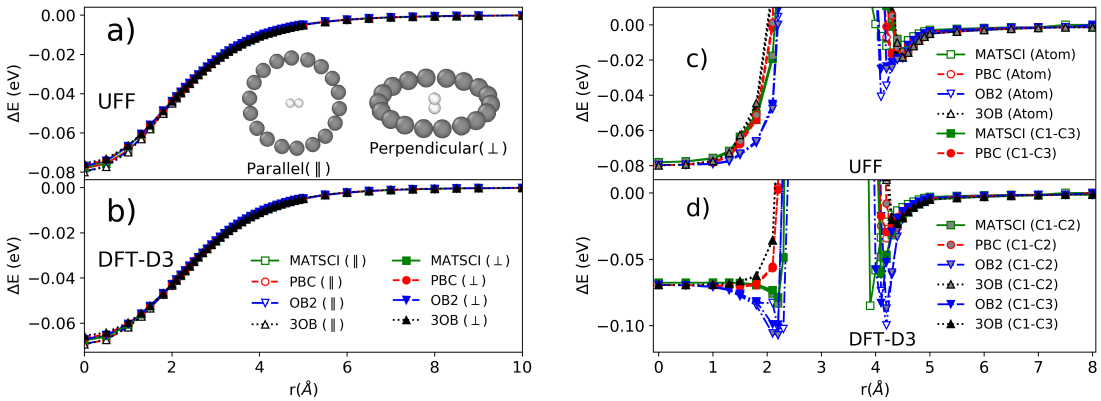


Figure 4: (Color on-line). Potential energy curves for the interaction of a $C_{18}$ with a $H_2$ molecule placed along the symmetry axis perpendicular to the ring plane and at the center of the carbon ring in a) and by considering three different adsorbate sites in b). The positions of the $H_2$ molecule center of mass follow straight lines to the different adsorbates site as shown in Fig 2 and 3. Hydrogen-hydrogen repulsion corrections are considered in the computation of the PECs. Similar results are obtained for perpendicular and parallel orientation of the $H_2$ molecule respect to the plane formed by the carbon ring. See text for discussion.

behavior with those obtained by UFF. The energy bonding is small and the $H_2$ molecule is not attracted to the carbon ring. Consequently, the formation of a $C_{18}H$ molecule can be feasible by dissociating the $H_2$ molecule through the collision dynamics (see below).

Consequently, the results presented for the OB2 and 3OB SK parameters are suitable to model the interaction of the $C_{18}$ molecule with molecular hydrogen and will be used to perform the quantum classical MD simulations. The later includes DFT-D3 dispersion corrections (hydrogen-hydrogen repulsion contributions).

### *3.2. Dynamical description*

#### *3.2.1. Atomic H projectiles*

In Fig. 5, we report the probability of adsorption and scattering of a hydrogen atom as a function of the impact kinetic energy. Standard error bars, as obtained by the statistics of our sampling, are included in the results. The obtained results by the Slater-Kirwood, UFF, and DFT-D3 dispersion corrections are similar for impact energies higher than 5 eV for OB2 (Fig. 5a) and 3OB (Fig. 5b) SK parameters. Note that the number of reflected and transmitted H atoms for impact energies higher than 5 eV is similar for both dispersion SK parameters. In this impact energy range, the interaction between the carbon ring and the H impact is negligible and the two methods report similar results. The OB2 MD simulations results show different behavior for the number of H atoms bound to the C ring due to the *sp* orbital hybridization. The 3OB simulations results are more stable with respect to the dispersion corrections included in these calculations. However, an important difference is observed at 2 eV where 40 % of the H atoms are bound for the OB2 MD simulations while 20 % of them form a $C_{18}H$ as obtained by the 3OB MD simulations. This can be understood from the PECs of these SK parameters (Figs. 2-3), where the potential well at the outer region of the carbon ring is deeper or wider for the OB2 SK parameters than those reported by the 3OB SK ones at the same interaction distances.

In Fig. 6 a), we show the position distribution of all the events of the H impacts that end up bound to the carbon ring at initial impact energy of 2 eV for the OB2 and 3OB MD with the inclusion of DFT-D3 dispersion corrections. We find that the most dominant final geometry of the $C_{18}H$ molecule is where one half of the original carbon ring is deformed by the presence of the hydrogen bound to the $C_{18}$ ring, while the second half of the ring preserves its original shape. This geometry is observed in all cases where $C_{18}H$ is formed regardless of the impact energy and SK parameters used in the MD simulations. This confirms that DFTB models properly the *sp*-hybridization of the valence electrons, which evolves from *sp* to $sp^2$

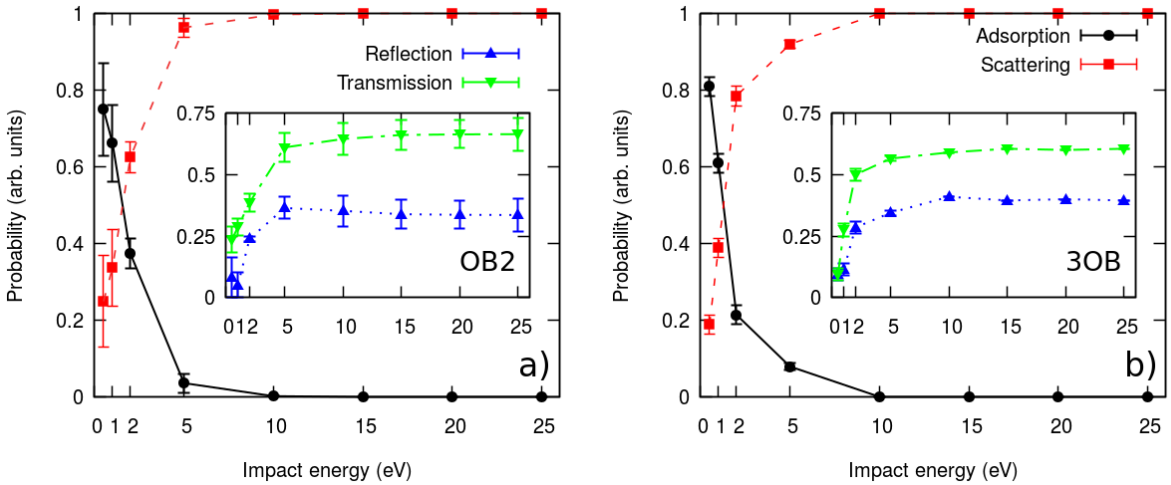


Figure 5: (Color on-line). Probability of adsorption and scattering of H projectiles, as a function of the impact energy, when irradiating a $C_{18}$ molecule by including the DFT-D3 dispersion corrections for OB2 parameters in a) and the 3OB SK ones in b). Probabilities of transmission and reflection of H projectiles are shown in the inset graph. Note that the probability of scattering $P_s = P_\beta + P_t$ with $P_{\beta,t}$ is the probability of reflection ($\beta$) or transmission ($t$) (See text for details).

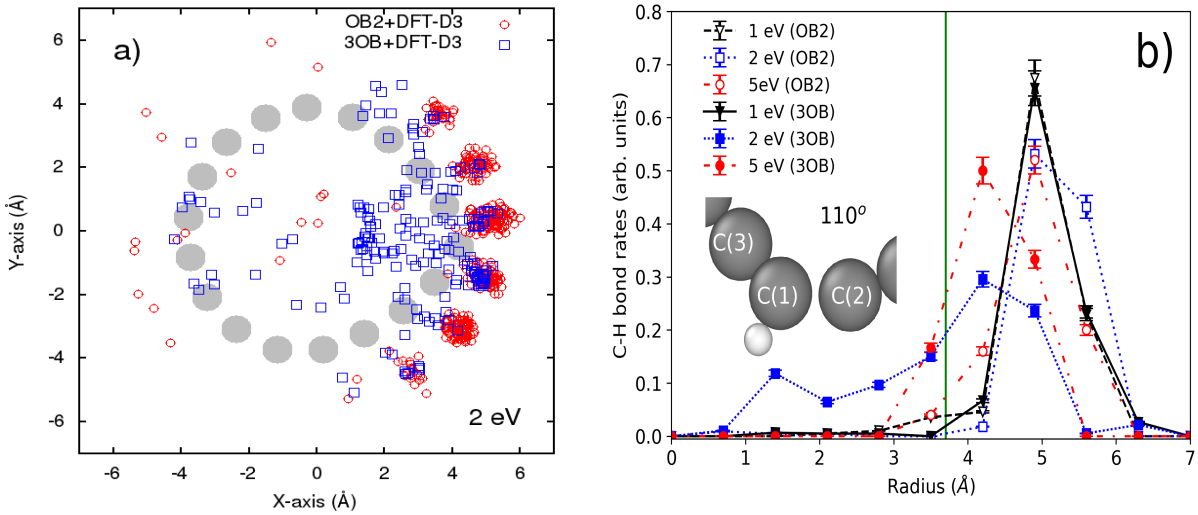


Figure 6: (Color on-line). a) Distribution of the final positions of H atoms bound to the carbon ring at 2 eV for OB2 and 3OB MD simulations with DFT-D3 dispersion corrections. We show the most common final geometry shape of the $C_{18}$ molecule when a H atom is bound to it. b) The average C-H bond rates as a function of their spatial position at 1, 2, and 5 eV for OB2 and 3OB MD simulations. The vertical green line at 3.75 Å depicts the radius of the $C_{18}$ molecule. The atomic geometry of the C-H bonding is depicted where the angle between the C(1)-C(2)-C(3) atoms is $\theta_t = 110^o$ (Carbon atoms are represented by grey spheres while a white sphere represents the hydrogen atom).

hybridization in the process of formation of $C_{18}H$. However, the distribution of H atoms bound to the carbon ring depends on the SK parameters used in the MD simulations. The H atom is more likely to be bound to the C ring outside and directly to a C atom, as follows from the PECs for the atomic case. On the other hand, the 3OB MD simulations show the formation of a $C_{18}H$ molecule with different position of the H atom: The H atom is sometimes bound to the C ring at the inside region, though still more likely to be bound at the external region. In Fig. 6 b), we report the C-H bond probabilities as a function of the distance $R = \sqrt{x^2 + y^2}$, where $x$ and $y$ are the final position of the H atoms bound to the carbon ring. As shown in Fig. 6a) for the 2 eV, OB2 MD simulations (hollow symbols) model the formation of the $C_{18}H$ molecule with a H atom bound outside for different impact energies. However, the 3OB MD simulations (solid symbols) agree well with those for OB2 at 1 eV. The H atom can also be bound to the C ring at the inside region for an impact energy of 5 eV according to the 3OB SK parameters. At 2 eV, the H atom can be found in a distance range of 1-5 Å. We notice that C atoms, in the $C_{18}H$ molecule, form an angle of $110^o$ between the three carbon atoms in the vicinity of the H atom, as shown in the inset of the figure. The C-H bonding modifies half of the geometry of the $C_{18}$ molecule due to *sp* hybridization. The visualization of the formation of the $C_{18}H$ molecule, by using 3OB SK parameters with DFT-D3 corrections, is provided in the supplementary material.

### *3.3. Molecular hydrogen irradiation*

In order to study the formation of a $C_{18}H_2$ molecule by molecular hydrogen irradiation, we define different events that are observed in our MD simulations: The first event is labeled as **Dyn. 1**, where the $H_2$ molecules are adsorbed by the carbon ring with the hydrogen atoms being bound to one or two neighboring C atoms. The formation of a $C_{18}H_2$ molecule is observed. In the second event called **Dyn. 2** the hydrogen molecules are dissociated and one H atom becomes bound to the carbon ring, while the second H atom is scattered. The formation of $C_{18}H$ molecules is found. In the third event named as **Dyn. 3**, kinetic energy of the projectile is high enough to break the bond of the $H_2$ molecule when irradiating the carbon ring. Here the hydrogen molecule is dissociated and scattered while the carbon ring remains in the initial geometry shape. Finally, the **Dyn. 4** case, where the most common event observed in our MD simulation is the repulsion of the $H_2$ molecule by the carbon ring without dissociating the $H_2$ molecule. This event is observed in the whole impact energy range, regardless the choice of the SK parameters and level of theory for the dispersion

corrections. The probabilities of the different events are computed as: $N_E/N_T$ where $N_E$ is the number of cases of each event and $N_T$ is the total number of $H_2$ molecules. The visualization of the dynamics of these events is included in the supplementary material.

In Fig. 7, we report results for the probability of adsorption and scattering of H atoms as a function of the impact energy for the OB2 and 3OB SK parameters in a) and b), respectively. The probabilities are calculated as follows: $N_p/N_{ta}$ with $N_p$ the number of scattered or adsorbed H atoms and $N_{ta}$ is the total number of H atoms (twice the number of $H_2$ molecules). In Fig. 7a), we notice that the $H_2$ molecule is not bound to the carbon ring for impact energies below 2 eV (lower panel), in agreement to the results for the PECs shown in Fig. 4b). H atoms are bound to the $C_{18}$ molecule in the impact energy range of 5 to 15 eV, where the $H_2$ impact has enough kinetic energy to break the 4.5 eV H-H bond. For impact energies higher than 2 eV, the scattered $H_2$ molecule can be dissociated and this event is dependent on the impact energy. However, one single H atom of the dissociated $H_2$ molecules is bound to the carbon ring in an impact energy range of 5-15 eV. The event **Dyn. 1** is only observed at 5 eV, where a H atom is first bound to one C atom, leaving the second H atoms free to travel around the carbon ring until it is bound to a C atoms at a symmetrical position respect to the first H atom. Fig. 7 b) shows the results obtained by performing MD simulations with 3OB SK parameters with DFT-D3 dispersion corrections and considering hydrogen bonding corrections. The results for scattered H atoms and molecules differ drastically with respect to those presented by OB2 SK parameters with UFF dispersion corrections. The probability of scattering reaches a minimum at 2 eV, which is also an important energy range for the atomic case. Probabilities for scattered H atoms do not significantly changes for impact energies higher than 2 eV. The probabilities for the **Dyn. 3** and **Dyn. 4** events are similar, where the dissociation of a H molecule and the reflection/transmission of a H molecule is possible at the same energies. However, the probability of a dissociated and scattered H

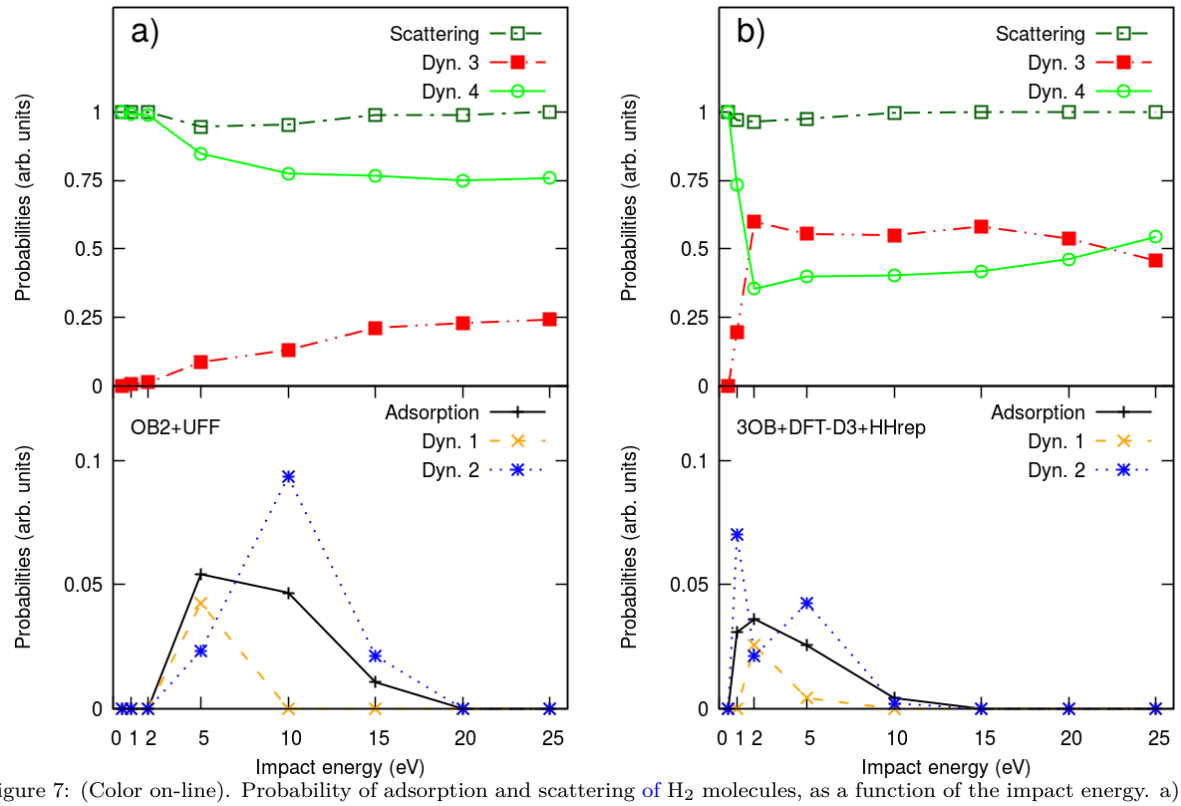


Figure 7: (Color on-line). Probability of adsorption and scattering of $H_2$ molecules, as a function of the impact energy. a) The results for the OB2-UFF approach and b) for the 3OB-DFT-D3 correction terms. Also shown are the probabilities of different events: adsorption of a $H_2$ molecule (**Dyn. 1**); adsorption of a H atom and H scattered (**Dyn. 2**); a $H_2$ molecule is dissociated and scattered (**Dyn. 3**); and a $H_2$ molecule is scattered (**Dyn. 4**).

molecule is bigger in an impact energy range of 2 to 20 eV. On the other hand, the formation of a $C_{18}H$ and $C_{18}H_2$ molecules is possible in an impact energy range of 1-10 eV. The OB3+DFT-D3 results present notable differences when compared to those for OB2+UFF calculations. The formation of a $C_{18}H_2$ molecule is observed at 5 eV for the latter and at 2 eV for the former. This is an effect of the inclusion of H-H repulsion contribution in the DFT-D3 dispersion corrections. Here, the molecule is formed when the $H_2$ molecule is dissociated with a H atom bound to a C atom and the second H atoms is bound to the first nearest neighbor C atom. A $C_{18}H$ can be formed at impact energies between 1 and 5 eV, as reported by the 3OB+DFT-D3 results.

In Fig. 8, we present all cases for the formation of a $C_{18}H_2$ molecule. In Fig 8 a), we show the results for the OB2+UFF and in Fig. 8 b) for 3OB+DFT-D3, according to the **Dyn. 1** and **Dyn. 2** events. Attention needs to be paid to the H atoms at the inside region of the carbon ring as the hydrogen atom is not located in the C ring. We also include the most common shape of the carbon ring at the final time of the MD simulations for both cases. Notice that the carbon ring is completely deformed by the binding of two H atoms for the OB2+UFF case. Interestingly, the H atoms are symmetrically bound to two different carbon atoms, one at one side of the ring and the other at opposite side. This produces a semi-elliptic shape of the $C_{18}H_2$ ring. Results for the 3OB+DFT-D3 case present a formation of the $C_{18}H_2$ molecule in a systematic way. The H atoms are bound to the first nearest C atom and the final shape of the carbon ring is barely affected. Only one half of the ring is deformed when the H atoms are bound to the C atoms. Besides, the H atoms are mainly bound to the C ring at the outside region, in good agreement with the atomic case. Of main importance is that we haven't observed fragmentation of the $C_{18}$ molecule by irradiation of hydrogen. This shows that the $C_{18}$ molecule ring is stable and thus a good candidate for hydrogen absorption or detection. The formation of $C_{18}H_2$ molecule suggests the use of the 3OB+DFT-D3 parameters for a study of the formation of a $C_{18}H_n$ molecule, with $n > 2$ in a cumulative process. This is work in progress and we will report its outcome elsewhere.

## 4. Concluding remarks

In this work, we performed numerical simulations with a molecular-dynamics approach based on the DFTB method to simulate irradiation by atomic and molecular hydrogen on a $C_{18}$ molecule (cyclo[18]carbon). We consider different sets of SK parameters to model the inter-atomic interaction between the C and H

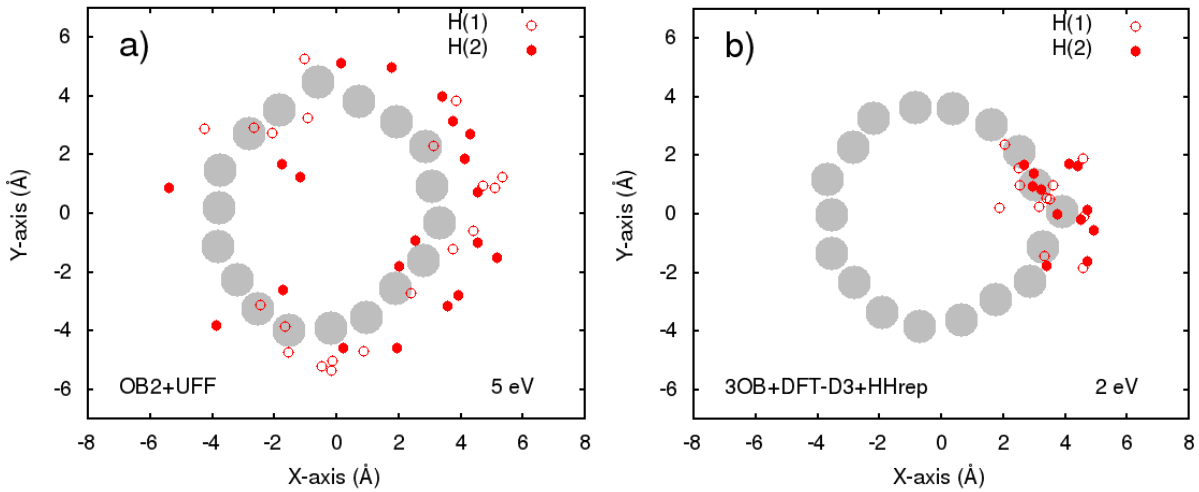


Figure 8: (Color on-line). Distribution of the final position of H atoms that form a $C_{18}H_2$ molecule, as obtained by OB2+UFF in a) and by 3OB+DFT-D3 in b) after irradiation by $H_2$. We include the most common final shape of the carbon ring. For the formation of $C_{18}H_2$ molecules, we differentiate the hydrogen atoms bound to the $C_{18}$ molecule according to the **Dyn. 1** event, where the $H_2$ is dissociated and the H atoms are bound to the carbon ring. The atoms that form the $H_2$ molecular projectiles are labeled as H(1) for the first H that is depicted by open circles and H(2) for the second H atoms illustrated by bullets.

atoms, as well as different approaches to include van der Waal interactions in our atomistic simulations by dftb+. We have used Slater-Kirwood polarizable atomic model, Lennard-Jones potential with Universal Force Field parameters, and the 3-body dispersion energy through a damped pairwise London-type factor correction in the DFTB approach. Potential energy curves (PECs) for the interaction of $C_{18}$ with atomic and molecular hydrogen at different adsorbate sites are computed to test the suitability of the DFTB parameters to properly model the physical and chemical physio-absorption process during the hydrogen irradiation on the carbon ring. These PECs also serve as a guide to understand the MD simulation results. For atomic irradiation, we found that the $C_{18}H$ molecule is more likely to be formed at impact energies below 10 eV, regardless the choice of the DFTB parameters and dispersion corrections. However the collision dynamics differ between the DFTB parameters at very low impact energies, where the H atom is mainly bound to the carbon at the outer region of the molecule for the case of the OB2 parameters. In contrast, the recently developed 3OB parameters model a $C_{18}H$ molecule with a H atom bound at the inner region for impact energies higher than 1 eV. For the molecular case, we found that the formation of a $C_{18}H_2$ molecule is feasible in an impact energy range between 2-15 eV. However differences are observed in the MD simulation results for OB2 and 3OB parameters. The formation of this molecule is only observed around 5 eV for the OB2 case and around 2 eV for the 3OB one. This disagreement is due to the inclusion of a DFT 3-body level of theory in the dispersion corrections and hydrogen-hydrogen repulsion corrections for the 3OB MD simulations with the DFT-D3 approach.

In conclusion, we find that the hydrogenation of $C_{18}$ by atomic and molecular hydrogen irradiation is highly probably at low irradiation energies in a single collision event. Work is in progress to study the feasibility of multiple hydrogen binding, either sequentially or in a cumulative process.

## Acknowledgments

FJDG acknowledges support from the A. von Humboldt foundation for research fellowship. RCT acknowledges support from DGAPA-UNAM PAPIIT-IN-111-820 and LANCAD-UNAM-DGTIC-228 as well as to the University of Heidelberg for its hospitality. CMF thanks CONACyT for the postdoctoral fellowship through the project FC-2016/2412. Results in this paper were obtained using the Seawulf institutional cluster at the Institute for Advanced Computational Science in Stony Brook University and the Max-Planck Computing and Data Facility.

## Appendix A. Supplementary material

We provide the raw data of the potential energy curves obtained by different SK parameters for the considered adsorbate cites, that are graphically reported in Sec 3.1. We also include the visualization of the formation of a $C_{18}H$ molecule at 2 eV by using the 3OB SK parameters with DFT-D3 dispersion correction, as well as the four different event observed during the hydrogen irradiation of the $C_{18}$ molecule by $H_2$ molecules.

## References

[1] Kaiser K, Scriven L M, Schulz F, Gawel P, Gross L and Anderson H L 2019 *Science* **365** 1299–1301 ISSN 0036-8075 (*Preprint* `https://science.sciencemag.org/content/365/6459/1299.full.pdf`) URL `https://science.sciencemag.org/content/365/6459/1299`

[2] Fowler P, Mizoguchi N, Bean D and Havenith R 2009 *Chemistry – A European Journal* **15** 6964–6972 (*Preprint* `https://onlinelibrary.wiley.com/doi/pdf/10.1002/chem.200900322`) URL `https://onlinelibrary.wiley.com/doi/abs/10.1002/chem.200900322`

[3] Hoffmann R 1966 *Tetrahedron* **22** 521 – 538 ISSN 0040-4020 URL `http://www.sciencedirect.com/science/article/pii/0040402066800200`

[4] Parasuk V, Almlof J and Feyereisen M W 1991 *Journal of the American Chemical Society* **113** 1049–1050

[5] Neiss C, Trushin E and Görling A 2014 *ChemPhysChem* **15** 2497

[6] Diederich F, Rubin Y, Knobler C B, Whetten R L, Schriver K E, Houk K N and Li Y 1989 *Science* **245** 1088

[7] Torelli T and Mitas L 2000 *Phys. Rev. Lett.* **85**(8) 1702–1705 URL `https://link.aps.org/doi/10.1103/PhysRevLett.85.1702`

[8] Arulmozhiraja S and Ohno T 2008 *The Journal of Chemical Physics* **128** 114301
[9] Silva Pereira Z and da Silva E Z 2020 *The Journal of Physical Chemistry A* **124** 1152–1157 pMID: 31971391 (*Preprint* https://doi.org/10.1021/acs.jpca.9b11822) URL https://doi.org/10.1021/acs.jpca.9b11822
[10] Baryshnikov G V, Valiev R R, Kuklin A V, Sundholm D and Ågren H 2019 *The Journal of Physical Chemistry Letters* **10** 6701–6705 pMID: 31609631 (*Preprint* https://doi.org/10.1021/acs.jpclett.9b02815) URL https://doi.org/10.1021/acs.jpclett.9b02815
[11] Stasyuk A J, Stasyuk O A, Solà M and Voityuk A A 2020 *Chem. Commun.* **56**(3) 352–355 URL http://dx.doi.org/10.1039/C9CC08399E
[12] Diederich F 1994 *Nature* **369** 199–207 URL https://doi.org/10.1038/369199a0
[13] Chen Z, Molina-Jirón C, Klyatskaya S, Klappenberger F and Ruben M 2017 *Annalen der Physik* **529** 1700056
[14] Hui L, Xue Y, Yu H, Liu Y, Fang Y, Xing C, Huang B and Li Y 2019 *Journal of the American Chemical Society* **141** 10677–10683
[15] Baughman R H, Eckhardt H and Kertesz M 1987 *The Journal of Chemical Physics* **87** 6687–6699 (*Preprint* https://doi.org/10.1063/1.453405) URL https://doi.org/10.1063/1.453405
[16] Gorter S, Rutten-Keulemans E, Krever M, Romers C and Cruickshank D W J 1995 *Acta Crystallographica Section B* **51** 1036–1045
[17] Rocca D, Gebauer R, Saad Y and Baroni S 2008 *The Journal of Chemical Physics* **128** 154105
[18] Aradi B, Hourahine B and Frauenheim T 2007 *The Journal of Physical Chemistry A* **111** 5678–5684
[19] Elstner M, Porezag D, Jungnickel G, Elsner J, Haugk M, Frauenheim T, Suhai S and Seifert G 1998 *Phys. Rev. B* **58**(11) 7260–7268
[20] 2019 http://www.dftb-plus.info/
[21] Gaus M, Goez A and Elstner M 2013 *Journal of Chemical Theory and Computation* **9** 338–354
[22] Elstner M, Jalkanen K J, Knapp-Mohammady M, Frauenheim T and Suhai S 2001 *Chemical Physics* **263** 203 – 219 ISSN 0301-0104
[23] Lukose B, Kuc A, Frenzel J and Heine T 2010 *Beilstein J. Nanotechnology* **1** 60 URL https://www.beilstein-journals.org/bjnano/articles/1/8
[24] Rauls E, Elsner J, Gutierrez R and Frauenheim T 1999 *Solid State Communications* **111** 459 – 464
[25] Vuong V Q, Akkarapattiakal Kuriappan J, Kubillus M, Kranz J J, Mast T, Niehaus T A, Irle S and Elstner M 2018 *Journal of Chemical Theory and Computation* **14** 115–125
[26] Novotny M, Dominguez-Gutierrez F J and Krstic P 2017 *J. Mater. Chem. C* **5**(22) 5426–5433 URL http://dx.doi.org/10.1039/C7TC00976C
[27] Dominguez-Gutierrez F J, Krstic P S, Irle S and Cabrera-Trujillo R 2018 *Carbon* **134** 189 – 198
[28] Domínguez-Gutiérrez F J, Martínez-Flores C and Cabrera-Trujillo R 2019 *Journal of Applied Physics* **125** 094506
[29] Vuong V Q, Akkarapattiakal Kuriappan J, Kubillus M, Kranz J J, Mast T, Niehaus T A, Irle S and Elstner M 2018 *Journal of Chemical Theory and Computation* **14** 115–125
[30] Martínez-Flores C, Domínguez-Gutiérrez F and Cabrera-Trujillo R 2020 *Radiation Physics and Chemistry* **166** 108513
[31] Slater J C and Kirkwood J G 1931 *Phys. Rev.* **37**(6) 682–697 URL https://link.aps.org/doi/10.1103/PhysRev.37.682
[32] Rappe A K, Casewit C J, Colwell K S, Goddard III W A and Skiff W M 1992 *J. Am. Chem. Soc.* **114** 10024
[33] Grimme S, Bannwarth C and Shushkov P 2017 *Journal of Chemical Theory and Computation* **13** 1989–2009
[34] Martyna G J, Tuckerman M E, Tobias D J and Klein M L 1996 *Molecular Physics* **87** 1117–1157
[35] Domínguez A, Niehaus T A and Frauenheim T 2015 *The Journal of Physical Chemistry A* **119** 3535–3544
[36] Řezáč J and Hobza P 2012 *Journal of Chemical Theory and Computation* **8** 141–151